CNRS
Centre National de la Recherche Scientifique

INFN
Instituto Nazionale di Fisica Nucleare

Preliminary VSR3 calibration (July 2010)

L. Rolland

VIR-0477A-10

August 4, 2010

VIRGO * A joint CNRS-INFN Project
Project office: Traversa H di via Macerata - I-56021 S. Stefano a Macerata, Cascina (PI)
Secretariat: Telephone (39) 50 752 521 – Fax (39) 50 752 550 – e-mail virgo@pisa.infn.it

Contents

1 Introduction

This note gives the status of the Virgo calibration in July 2010 for the start of the Virgo 3rd Science Run, VSR3. The calibration data were taken during the weeks before the run, from June 19th to August 4th 2010[1].

The methods are the same as described in [1] and [2]. The modifications of the interferometer (ITF) configuration related to the calibration between the end of VSR2 and the start of VSR3 are the following:

1. modification of the timestamp associated to the ADC data packets. See appendix C of [1] for the configuration during VSR2. Since January 19th 2010[2], it is the time of the first sample of the ADC board. For ADCs sampling all signals at 20 kHz, the timestamp of the packet is advanced by 1.7 μs compared to VSR2 data.

2. on July 15th 2010, modification of the PAGE_DELAY in the DAQ for all the ADC with data at 20 kHz: from -50 to -48 μs.

3. installation of the monolithic suspensions for the arm mirrors: the mirrors and reference masses have been changed. The mirror actuation response are thus different. In particular, the new reference masses have Aluminium around the coil instead of stainless steel. This should reduce the effect of Eddy current and flatten the actuation responses.

4. installation of the new coil drivers on the NI and WI suspensions[3].

5. installation of the new DSPs on all the suspensions. This should not have impact on the calibration.

6. use two additionnal photodiodes at the ITF output port to build the signal Pr_B1_ACp. The two additionnal channels Pr_B1_d4,5_ACp are not sampled in the same ADC as the channels Pr_B1_d2,3_ACp.

The association of modifications 1 and 2 induced no change in the way the data are stored in the frames compared to VSR2.

2 Dark fringe sensing

A synoptic of the general sensing of the dark fringe channels is shown in the figure 1 of [1].

[1] Stored in file with calibration period 961000000_966000000.

[2] logbook entry 26323

[3] in April 2010, see logbook entries 26639 and 26699 for WI, 26650 and 26701 for NI. The filters in the DSP were updated in July 2010. The voltage monitoring channels (i.e. Ca_NI_RM_CoilU) have been added on July 22th 2010, see logbook entry 27122.

2.1 Pr_B1_ACp channels

The sensing and timing of the raw channels $Pr\_B1\_d\{2,3,4,5\}\_ACp$ are first studied. The sensing of the combined channel Pr_B1_ACp is then discussed.

2.1.1 Readout of the raw channels $Pr\_B1\_d\{2,3,4,5\}\_ACp$

As during VSR2, the readout of the raw channels $Pr\_B1\_d\{2,3,4,5\}\_ACp$, sampled at 20 kHz, are done through the following path, without emphasis filters:

- photodiode sensing,
- demodulation electronics (analog),
- digitization by an ADC. The ADC board has an analog filter (a 6th order Butterworth filter cutting at 100 kHz, in the so-called mezzanine) which induces a measured delay of $(6 \pm 0.5)\,\mu$s. The signal is then sampled at 800 kHz. An analog 8th order Butterworth anti-alias filter ($f_0 = 7503.65$ Hz) is used before the signal is subsampled at 20 kHz, picking 1 sample over 40 (the last sample over the 40 of the window is kept).
- the DAQ where some delay can be adjusted before the data are stored: set to $-48\ \mu$s such that the samples of the 20 kHz channels are stored in the corresponding frame.

Below 2 kHz, the 8th order Butterworth filter is equivalent to a pure delay of $(109 \pm 1)\ \mu$s (see [1], figure 2).

Note that the signals from $d4$ and $d5$ photodiodes are sampled in a different ADC board than the signals from $d2$ and $d3$.

2.1.2 Measurement of the delay of the sensing of $Pr\_B1\_d\{2,3,4,5\}\_ACp$

It has been checked that the delay of the channels $Pr\_B1\_d\{2,3\}\_ACp$ did not change since VSR2 (using the signal $Ti\_1PPS\_GPSMaster$ sampled on the same ADC board).

(See channel $Ti\_1PPS\_GPSMaster\_t0$ after July 30th 2010.)

In order to check the timing of the $d4$ and $d5$ photodiodes, the TFs of $Pr\_B1\_d\{4,5\}\_ACp/Pr\_B1\_d2\_ACp$ have been measured. The delay between the channels is estimated from the phase of the TFs where some coherent noise is seen by all the photodiodes[4]. Observed differences are lower than $1\,\mu$s, well within systematic errors.

2.1.3 Models of $Pr\_B1\_\{d2,d3,d4,d5\}\_ACp$ sensing

To conclude about the raw channel sensing, two models can be defined. They are given in the table 1.

[4] at calibration line frequencies, and at higher frequencies during a period where sensitivity was limited by phase noise (GPS 964518010)

Model up to 20 kHz - The readout of the $Pr\_B1\_\{d2, d3\}\_ACp$ channel up to 20 kHz can be modeled by:

- a 8th order Butterworth filter with frequency 7503.65 Hz,
- a delay of -59.7 ± 5 μs ($49.3 - 109$ μs)

Simple model up to 2 kHz - Considering this response only below ~ 2kHz, it can be modeled by a simple delay of $49.3 \pm 4\,\mu$s as measured above.

2.1.4 Delay of the sensing of Pr_B1_ACp

The Pr process makes the sum of the raw signals from the photodiodes, $Pr\_B1\_d2, 3, 4, 5\_ACp$, in V, to compute the main channel Pr_B1_ACp, in W. The computation delay of the Pr process, of 100 μs, is corrected for in the Pr output channel. The TF from the raw channels, converted into watt with the same parameters as in the online process, to the main channel has been computed:

$$\frac{Pr\_B1\_ACp}{0.0004354 \times d2\_ACp + 0.0005879 \times d3\_ACp + -0.0004157 \times d4\_ACp + 0.0004157 \times d5\_ACp}$$

It is shown figure 1: as expected, no delay is introduced by the Pr process. The model for the sensing of Pr_B1_ACp is thus the same as for the raw channels and is given in table 1.

2.2 The sensing of the channels $Pr\_B1p\_\{DC, ACp, ACq\}$

The Pr_B1p raw channels are used to reconstruct ΔL in free swinging Michelson data. The knowledge of its sensing is thus very important since it is included in the raw measurements of the mirror actuation TF and has to be subtracted to get the mirror actuation itself. Two photodiodes $d1$ and $d2$ are used to measure the Pr_B1p signals but their signals are not summed. The channels $Pr\_SW\_B1p\_DC$ and $Pr\_SW\_B1p\_AC$ indicate what photodiode is used to compute the channels $Pr\_B1p\_\{DC, ACp, ACq\}$: 0 means $d1$, 1 means $d2$.

2.2.1 The sensing of the raw channels $Pr\_B1p\_\{d1, d2\}\_\{DC, ACp, ACq\}$

The Pr_B1p raw channels ($d1$ and $d2$) are sampled at 20 kHz by the same ADC as the $Pr\_B1\_d2, d3$ raw channels at 20 kHz described in the section 2.1.3. A similar readout path is defined, also without emphasis filter. The same models can thus be defined (see table 1).

2.3 Time jitter of the timing system

The measurement of the timing jitter has been added in the TiMoni server. The online measurement is stored in the channel Ti_10MHz_Delay.

The spectrum of the delay is the same as during VSR2. The interested part to be looked at is above 1 Hz since the ADC clock is synchronise on the IRIG-B clock every second. Above 1 Hz, the estimated timing jitter is below $0.1\,\mathrm{ns}/\sqrt{\mathrm{Hz}}$, orders of magnitude below the calibration timing uncertainties.

2.4 Tables

Parameters	Full model ($f < 20\,\mathrm{kHz}$)	Simple model ($f < 2\,\mathrm{kHz}$)
Gain	1	1
Φ_0 (rad)	0	0
Delay (μs)	-59.7	49.3
Butterworth frequency (Hz)	7503.65	–

Table 1: ***Models for the sensing of the*** $Pr\_B1\_\{d2, d3, d4, d5\}$**,** Pr_B1 ***and*** $Pr\_B1p\_\{d1, d2\}$ ***channels at 20 kHz.*** *The delays are given related to the absolute GPS time.* **Simple model***: the delay has been measured with the ramped 1 PPS. It is valid up to 2 kHz.* **Full model***: the delay is the simple model delay subtracted for the Butterworth equivalent delay. It is valid up to 20 kHz. Systematic errors are* ± 4 μs *on the delay.*

2.5 Figures

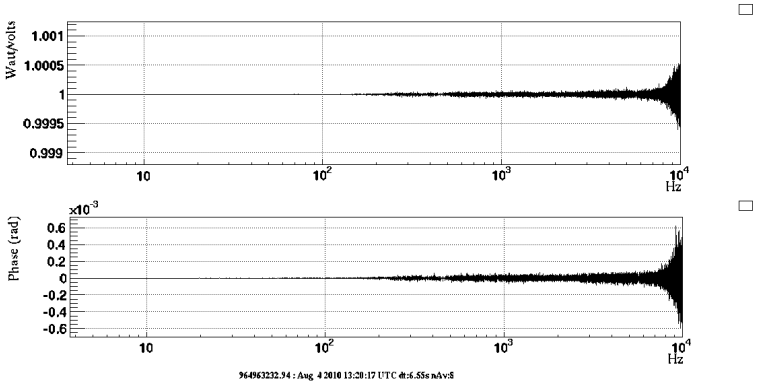

Figure 1: TF of the main channel Pr_B1_ACp *to the weighted sum of the raw channels* $Pr\_B1\_d2, 3, 4, 5\_ACp$.

3 Calibration of the mirror actuation

The mirror actuation is defined as the TF (with modulus in m/V) from the correction signal to the induced mirror motion. The time reference is the GPS time.

In the plots that are shown, the actuation is corrected for the mechanical model of the pendulum, defined as a 2nd order low-pass filters with $f_0 = 0.6\,\mathrm{Hz}$ and $Q = 1000$.

3.1 Description of the measurements

3.1.1 Actuation in HP mode: Free Michelson data

The mirror actuation is measured in High Power (HP) mode using free swinging Michelson data.

Due to the new mirrors, the contrast of the asymmetric Michelson configurations used for the calibration has descreased. This lower contrast reduced the sensitivity to the mirror motion ΔL at high frequency.

During VSR2, the demodulation phase of Pr_B1p was not tuned for the Michelson data. Since June 2010, it has been set to $-20°$ such that Pr_B1p_ACq is close to 0 and Pr_B1p_ACp is close to its maximum amplitude. This way, the sensitivity in ΔL is improved reconstructing it using $Pr\_B1p\_d2\_ACp$.

The reconstruction method has been recently adapted and improved:

- the raw channels are used: $Pr\_B1p\_d1\_DC$ and $Pr\_B1p\_d2\_ACp$. An offset had to be taken into account for the ACp signal also[5].
- all the information from the ellipse fit are used when extracting its widths and position, including the ellipse orientation and size[6].
- a first pass on the data is used to fit the ellipse and a second path on the data is then used to compute ΔL from the parameters of the ellipse fitted on the current data[7].
- the ellipse parameters are low-passed using a sliding average computed using all the samples at 20 kHz[8].

Two examples of ellipse $Pr\_B1p\_d2\_ACp, ACq$ vs $Pr\_B1p\_d1\_DC$ and of ΔL spectrum are shown in figure 2.

[5] When using Pr_B1_ACp, q, they were considered as centered on 0.

[6] Before, the ellipse main axis were supposed to be along the DC and AC signals.

[7] Before, the ellipse was fitted at t_f using the data between t_{f-1} and t_f, and these parameters were used to compute ΔL on the data from t_f to t_{f+1}

[8] Before, a sliding average was computed, but only when the parameters were estimated (ellipse fit), not in-between.

Note that the contrast estimated from the ellipse is of the order of 0.08 while it was around 0.21 during VSR2. This lower contrast (in agreement with the change of mirrors) reduced the sensitivity to ΔL at high frequency.

The measured TF is then $\Delta L/zMir$. Only the data with coherence higher than 70% have been used and are shown in the figures (section 3.4). Since one wants to measure the mirror actuation A from the correction signal (i.e. Sc_WE_zCorr) to the mirror motion, this TF is corrected for (see note [3]):

1. the pendulum mechanical response P: a second order low-pass filter[9] with frequency $f_0 = 0.6$ Hz and quality factor $Q = 1000$,
2. the light propagation time: 0 μs for NI and WI, 10 μs for NE and WE, 0 μs for BS in NE-WI configuration and 10 μs for BS in WE-NI configuration,
3. the delay from PrCa to the mirror actuation DSP: 100 μs,
4. the delay induced by the readout of $Pr\_B1p\_\{d1, d2\}\_\{DC, ACp, ACq\}$. The absolute delay is 49.3 μs below 2 kHz (see table 1).

The first two corrections are done automatically in the calibration code. In the following, the plots of A are corrected for these two effects only. In the tables, this delay is given as the "raw delay". The last two delays ($100 + 49.3 = 149.3$ μs) are taken into account afterwards to get the true delay of the actuation A, also given in the tables. The delay is thus the absolute delay between the correction signal as stored in the Virgo data and the GPS time.

3.1.2 LN1/HP actuation ratio measurements

A set of measurements has been taken. The configuration and excitation signals were the same as during VSR2. The data with coherence above 80% are shown in the figures (section 3.4).

3.1.3 Mirror actuation in LN1 mode

The mirror actuation in LN1 mode is obtained multiplying the mirror actuation in HP mode (measured in free swinging Michelson data) by the LN1/HP ratio. The multiplication is done using the data points measured at the free Michelson line frequencies. The data are then fitted by a model including poles and zeros.

As for the actuation in HP mode, the plots of A are not corrected for some delays. Both the "raw delay" (only corrected for the light propagation time) and the corrected delay are given in the tables with the model parameters.

[9] The mechanical response of the pendulum is modeled by: $P(f) = \frac{-f_0^2(f^2-f_0^2)-j\frac{f_0^3 f}{Q}}{(f^2-f_0^2)^2+(\frac{f f_0}{Q})^2}$. It is equivalent to write it as function of $s = \mathrm{j}\omega$ as: $P(s) = \frac{\sum_{i=0}^{2} a_i \times s^i}{\sum_{k=0}^{2} b_k \times s^k}$ with $a_2 = a_1 = 0$, $a_3 = 14.2122$, $b_2 = 1$, $b_1 = 0.00376991$ and $b_0 = 14.2122$.

3.2 Actuation calibration

The parameters of the parameterizations fitted on the mirror actuation measurements are given in the table 3 for the configurations used in the longitudinal controls and in the table 4 for the configurations used for the hardware injections.

The figures of the different data and fit are shown in the section 3.4.

3.2.1 Actuation in HP mode

Free swinging Michelson data were analysed to extract the actuation response A in HP mode.

The arm payloads have been changed in Spring 2010. The new mirror reference masses are made of Aluminium, and Eddy currents are expected to be much lower than before. As a consequence, the measured actuation response are much flatter than before, which confirms our hypothesis that the Eddy currents were the cause of the non flat response of the actuation.

3.2.2 LN1 to HP TF ratio

Shape of the ratio - In HP mode, the voltage input is converted in a current in the coil through a trans-conductance amplifier. It response is not well known but is expected to be rather flat up to a few kHz. Introduce a delay ?

In LN modes, the voltage input is converted to a current through serie resistors. These resistors R_s are in serie with the inductance $L_c \sim 5\,\mathrm{mH}$ of the coil[10], while it was around 3.3 mH on the previous payloads.

The conversion voltage to current by the coil driver is thus a pole at frequency $f_p = \frac{R_s}{2\pi L_c}$. In LN1 mode, the serie resistors include the so-called serie resitors themselves ($300\,\Omega$), the protection resistor ($10\,\Omega$) and the coil internal resistor ($\sim 5\,\Omega$). The pole is thus around 10 kHz, far above the measurements. Below a few Hz, it is equivalent to a delay of $\sim 16\,\mu$s.

Different DACs are used in HP and in LN1 modes. The anti-imaging filters might be slightly different between both channels. The cut-off being around 3 kHz, it should not be visible below 1 kHz in the modulus. Below 1 kHz, the equivalent delay of the DAC filters is $177 \pm 5\,\mu$s. Differences of the order of $10\,\mu$s could arise between different DACs [4].

The ratio is thus expected to be close to flat up to 1 kHz. Some mistuning in the compensation of the de-emphasis filters (0.9 Hz and 9Hz) can explain a few percent variations in modulus ratio below a few tenth of Hz and of the order of 30 mrad variations in phase difference below a hundred Hz.

The modulus of the LN1 to HP ratio are flat within 5% up to 1 kHz. The phase difference shows some behaviour below 100 Hz that must be due to the filter compensation tuning. At higher frequency, it can be interpreted as a delay.

[10] see logbook entry 26630

3.2.3 Actuation response in LN1 mode

Difference between coils - The ratio is different for the up and down coils. This might induce systematic errors since their average is used when computing the WE actuation in LN1 mode from the actuation in HP mode.

3.3 Tables

Parameter	Values	Names of real pulsations
7 zeros (rad/s)	-268.962	z_1
	$-\mathrm{j}\times 53346.9$ and $+\mathrm{j}\times 53346.9$	z_2
	$-\mathrm{j}\times 65336.3$ and $+\mathrm{j}\times 65336.3$	z_3
	$-\mathrm{j}\times 117520$ and $+\mathrm{j}\times 117250$	z_4
8 poles (rad/s)	-31423.2	p_1
	$-21492-\mathrm{j}\times 10099.1$ and $-21492+\mathrm{j}\ times 10099.1$	p_2, p_3
	$-13768-\mathrm{j}\times 19533.1$ and $-13768+\mathrm{j}\ times 19533.1$	p_4, p_5
	$-4416.78-\mathrm{j}\times 22931.4$ and $-4416.78+\mathrm{j}\ times 22931.4$	p_6, p_7
	-266.764	p_8

Table 2: ***Model of the 8th order anti-alias filter of the DAC between the DSP and the coil driver****. The full expression of the associated TF is given in appendix B.6.*

		WE, U-D coils	NE, U-D coils	BS, four coils
LN1	Gain (μm/V)	15.014 ± 0.02	16.98 ± 0.023	89.84 ± 0.05
	Raw delay (μs)	(426.5 ± 3.5)	(419.9 ± 2.7)	(372.5 ± 1.8)
	Delay (μs)	277.2 ± 3.5	270.5 ± 2.7	223.2 ± 1.8
	Φ_0 (rad)	0	0	π
	Pole frequency (Hz)		–	3113.9 ± 88
	DAC anti-alias filter	See model in table 2		
	Pendulum	One 2nd order low-pass filter: $f_0 = 0.6$ Hz, $Q = 1000$		
	χ^2/ndf	40.8/26	5.8/24	60.8/23

Table 3: ***WE (U-D coils), NE (U-D coils) and BS (four coils) mirror actuation parameterizations****, in HP mode and LN1 mode. The models are valid up to 1.0 kHz. The χ^2/ndf of the fits are given. The raw delay is the measured delay that includes the delay from the injection path to the DSP and the delay from the Pr_B1p channels sensing. The corrected delay takes as reference the correction channel in the DSP (i.e. Sc_WE_zCorr) and does not contain the B1 sensing delay nor the delay for the injection part (raw delay with 100 μs less for the PrCa to DSP delay and 49.3 μs less from the dark fringe sensing: delay = raw_delay − 100 − 49.3 μs). Applying these TFs to zCorr should enable to estimate the induced motion at absolute GPS time.*

		WE, L-R coils	NE, L-R coils
LN1	Gain (μm/V)	15.16 ± 0.014	17.06 ± 0.023
	Raw delay (μs)	(599.9 ± 3.0)	(594.3 ± 2.5)
	Delay (μs)	650.6 ± 3.0	645.0 ± 2.5
	Φ_0 (rad)	0	0
	Pendulum	One 2nd order low-pass filter: $f_0 = 0.6\,\mathrm{Hz}$, $Q = 1000$	
	χ^2/ndf	45.3/26	23.3/26

Table 4: ***WE (L-R coils), NE (L-R coils) mirror actuation parameterizations****, in HP mode and LN1 mode. The WE actuations model are valid up to 1.0 kHz. The* χ^2/ndf *of the fits are given. The raw delay is the measured delay that includes the delay from the injection path (from PrCa) to the DSP and the delay from the* Pr_B1p *channels sensing. The corrected delay takes as reference the channels sent by the CaInjectors (i.e.* Ca_WE_zMirLR*) and does not contain the B1 sensing delay (raw delay with 100* μs *more since the hardware injections are done from the CaInjectors and* 49.3 μs *less from the dark fringe sensing:* $delay = raw\_delay + 100 - 49.3$ μs*). Applying these TFs to* Ca_WE_zMirLR *channels should enable to estimate the induced motion at absolute GPS time. In order to simplify the model set in the hardware injection system, the complete model for the DAC anti-alias filter has not been included.*

3.4 Figures

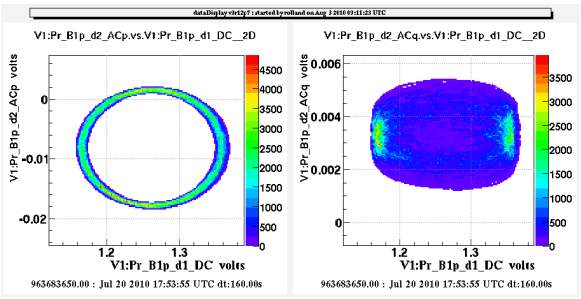

(a) GPS 930344269, 3 min.

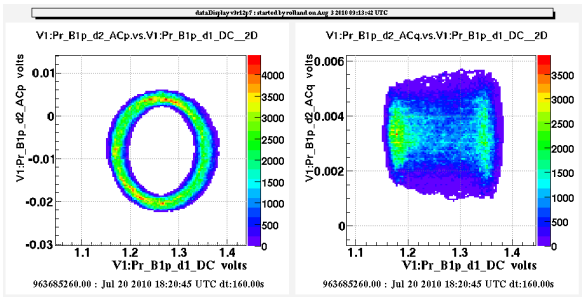

(b) GPS 930346691, 3 min.

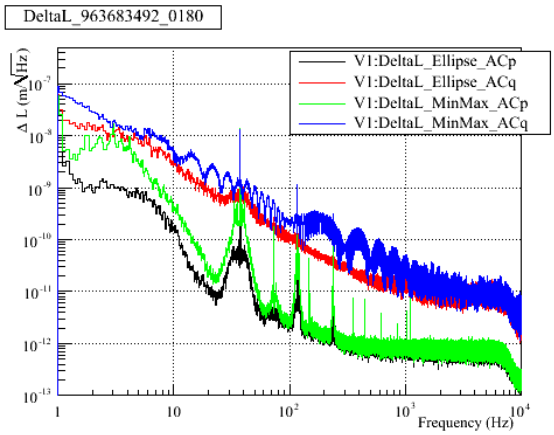

(c) GPS 963683492, 3 min.

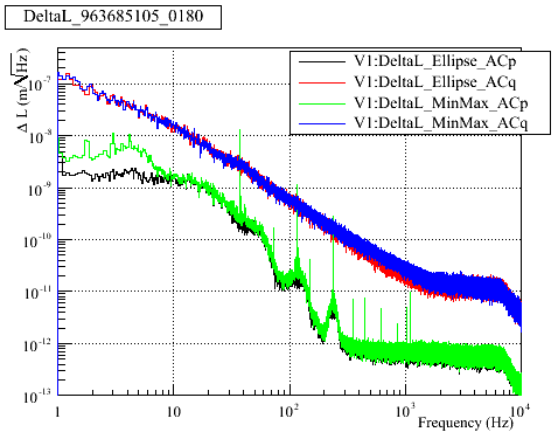

(d) GPS 963685105, 3 min.

Figure 2: ***Left: typical measured ellipses*** *Pr_B1p_d2_ACq* ***vs*** *Pr_B1p_d1_DC* ***and*** *Pr_B1p_d2_ACp* ***vs*** *Pr_B1p_d1_DC.* ***Right: typical reconstructed*** ΔL ***from free swinging Michelson data.*** *The channel* ΔL*_Ellipse_ACp (black) is used for the actuation calibration.*

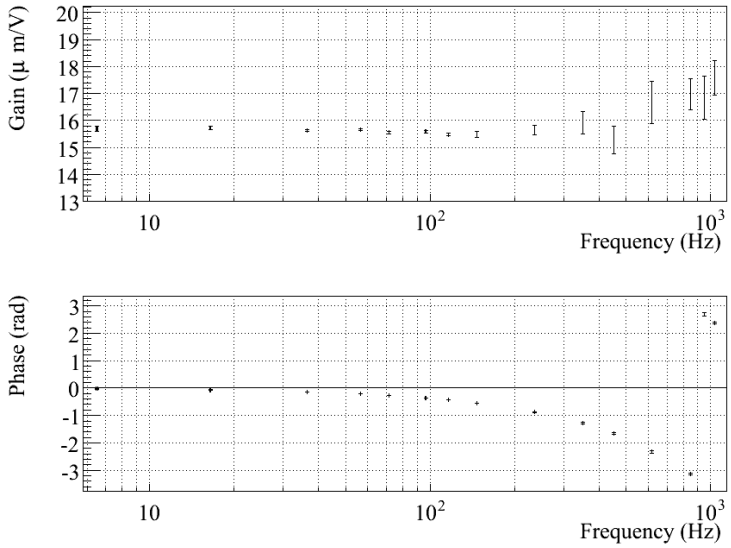

Figure 3: ***Measured actuation of the WE mirror using the U-D coils in HP mode****, fitted model and residuals.*

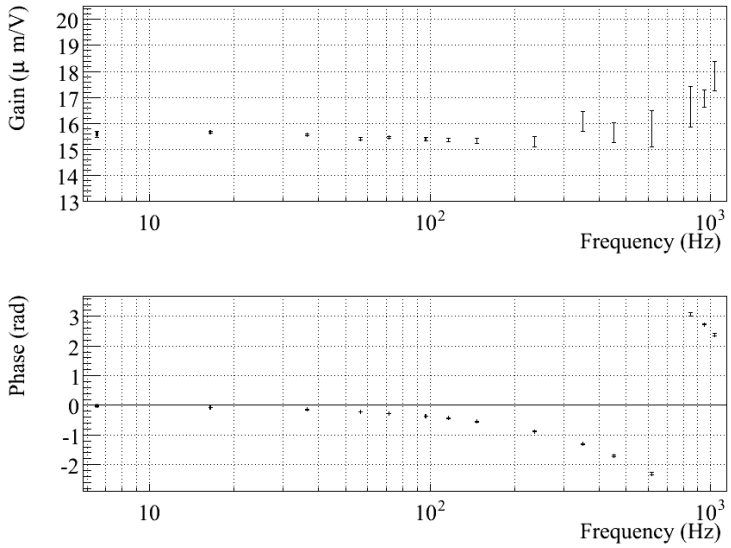

Figure 4: ***Measured actuation of the WE mirror using the L-R coils in HP mode****, fitted model and residuals.*

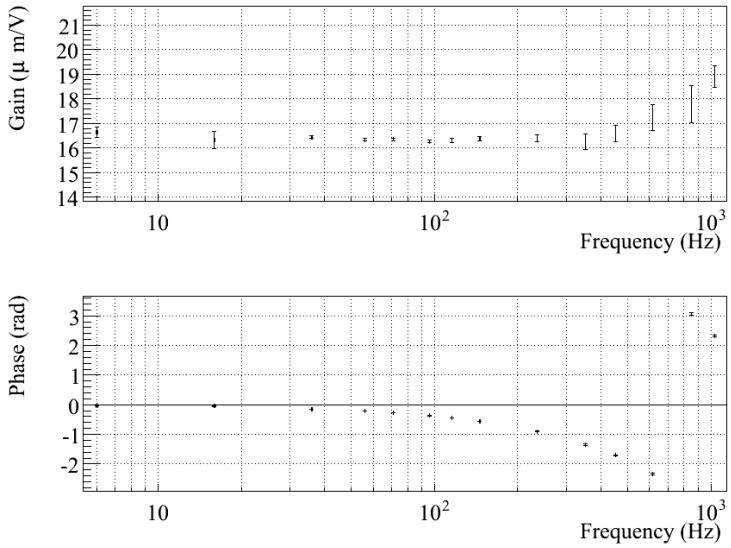

Figure 5: ***Measured actuation of the NE mirror using the U-D coils in HP mode****, fitted model and residuals.*

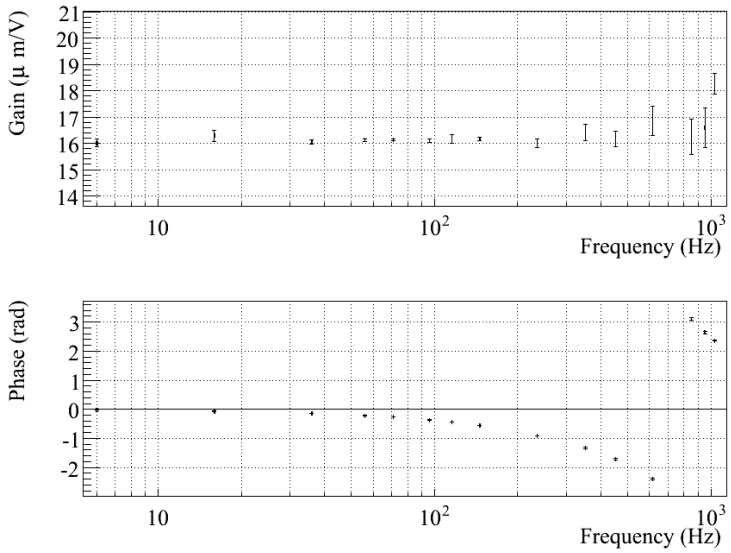

Figure 6: ***Measured actuation of the NE mirror using the L-R coils in HP mode****, fitted model and residuals. The data have been fitted up to 400 Hz only.*

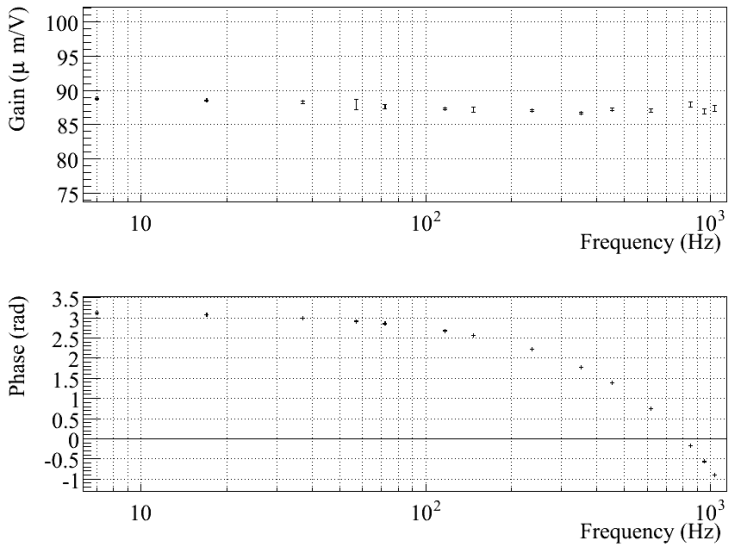

Figure 7: ***Measured actuation of the BS mirror using the four coils in HP mode****, fitted model and residuals.*

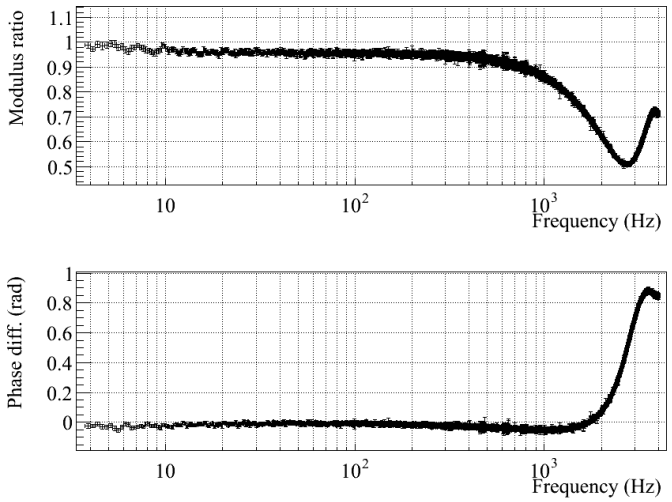

(a) Coil Up, averaged

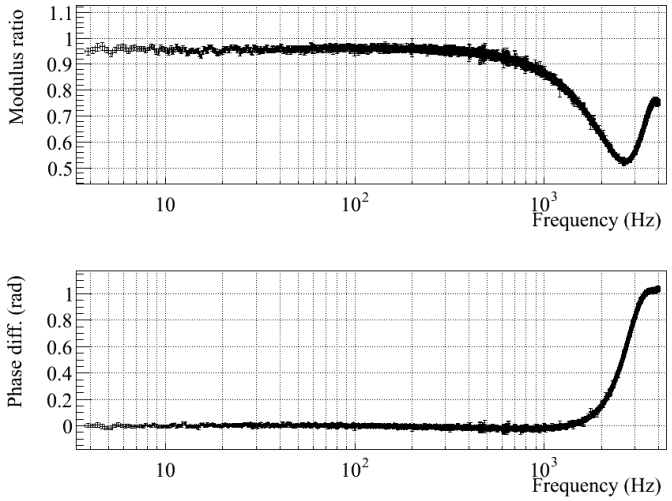

(b) Coil Down, averaged

Figure 8: ***Measured actuation TF ratio (LN1/HP) for the up and down coils of the WE mirror.***

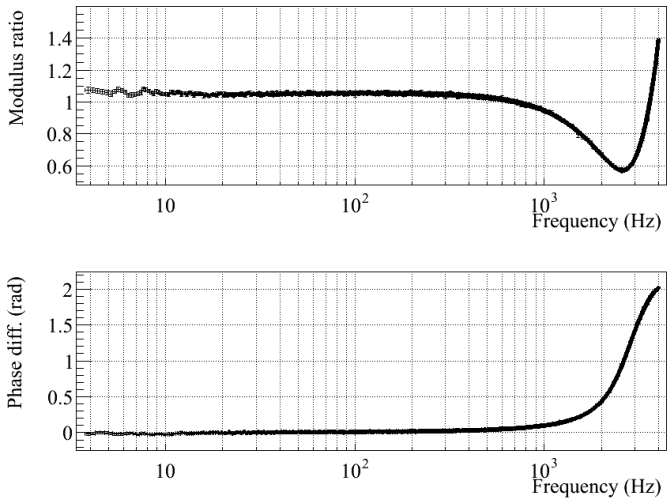

(a) Coil Up, averaged

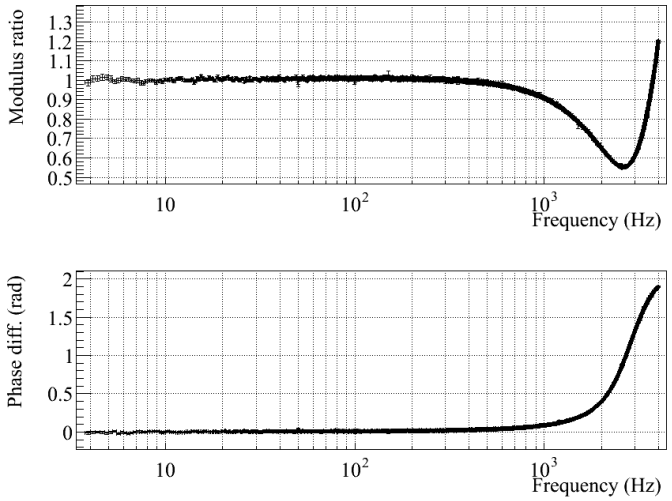

(b) Coil Down, averaged

Figure 9: ***Measured actuation TF ratio (LN1/HP) for the up and down coils of the NE mirror.***

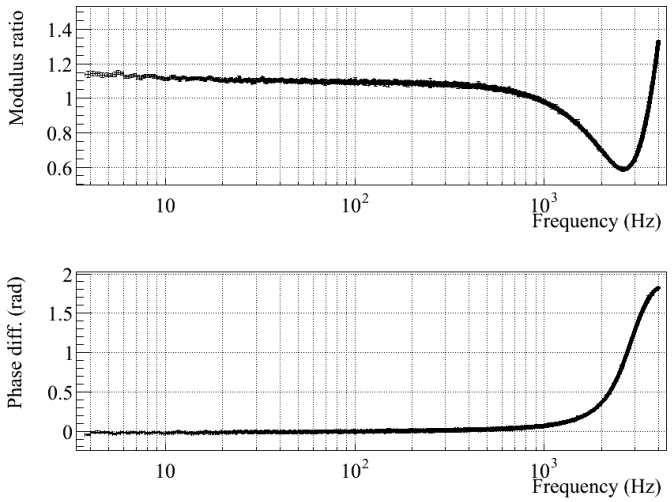

(a) Coil Left, averaged

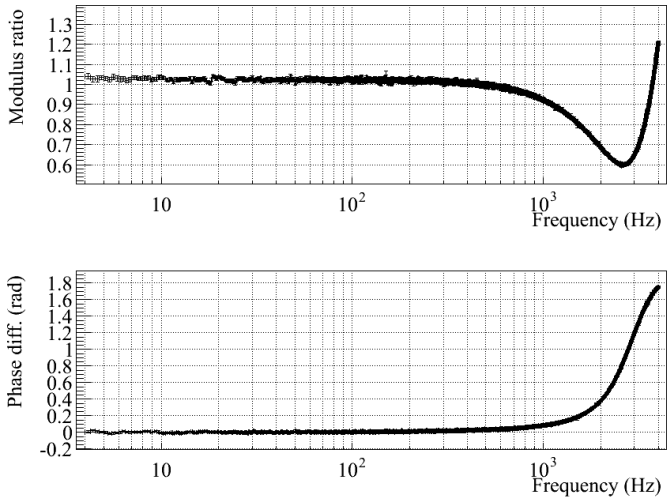

(b) Coil Right, averaged

Figure 10: ***Measured actuation TF ratio (LN1/HP) for the left and right coils of the NE mirror.***

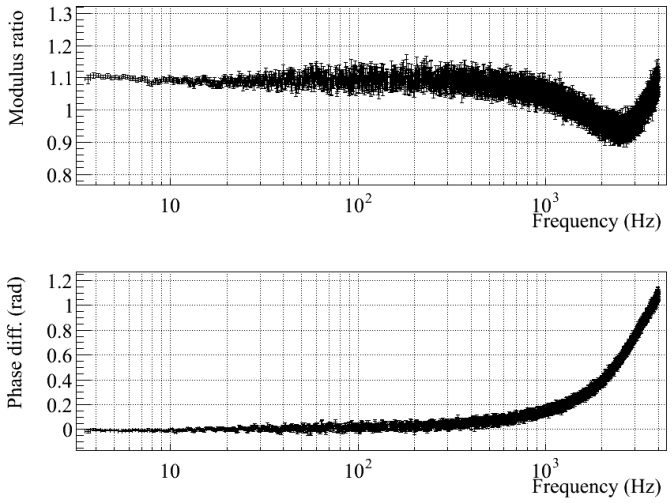

(a) Coil Up-Left, averaged

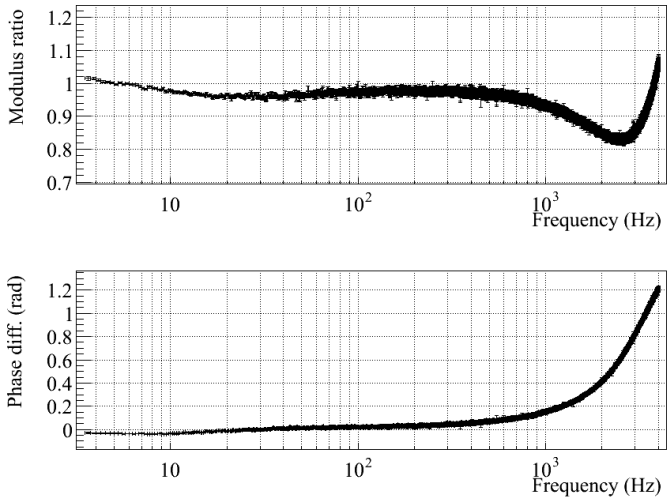

(b) Coil Up-Right, averaged

Figure 11: ***Measured actuation TF ratio (LN1/HP) for the up-left and up-right coils of the BS mirror.***

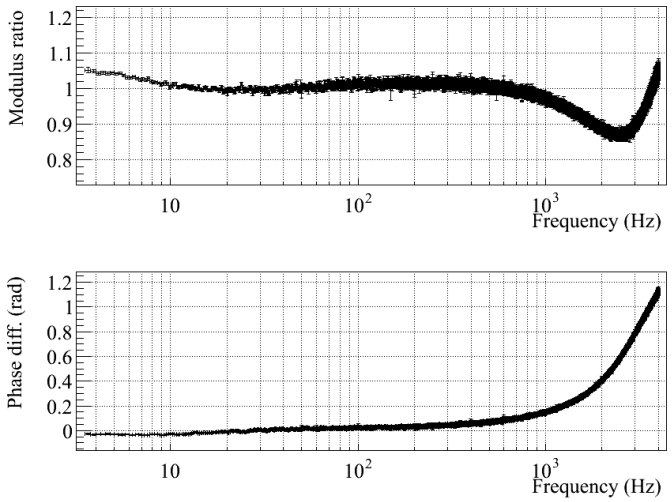

(a) Coil Down-Left, averaged

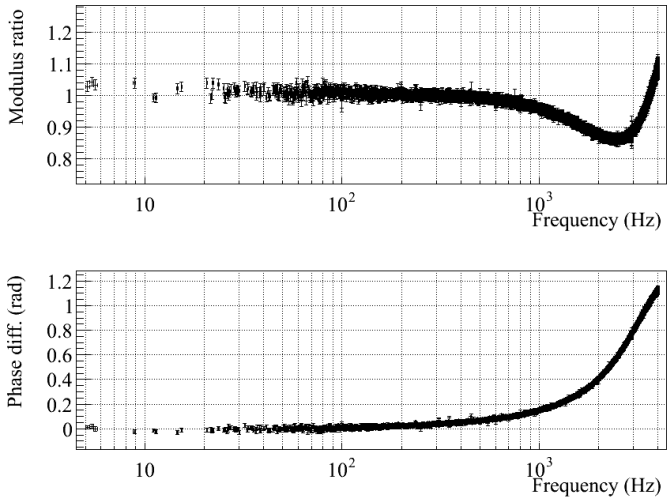

(b) Coil Down-Right, averaged

Figure 12: ***Measured actuation TF ratio (LN1/HP) for the down-left and down-right coils of the BS mirror.***

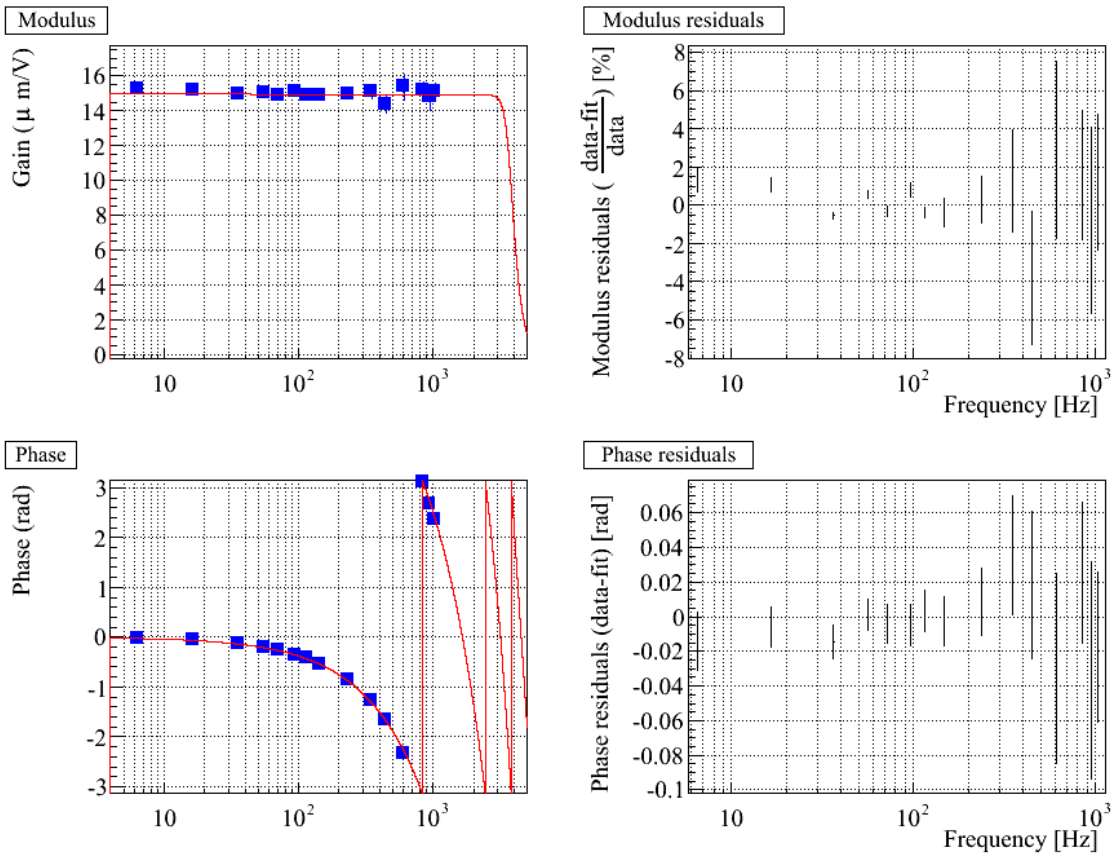

Figure 13: ***Measured actuation of the WE mirror using the U-D coils in LN1 mode****, fitted model and residuals.*

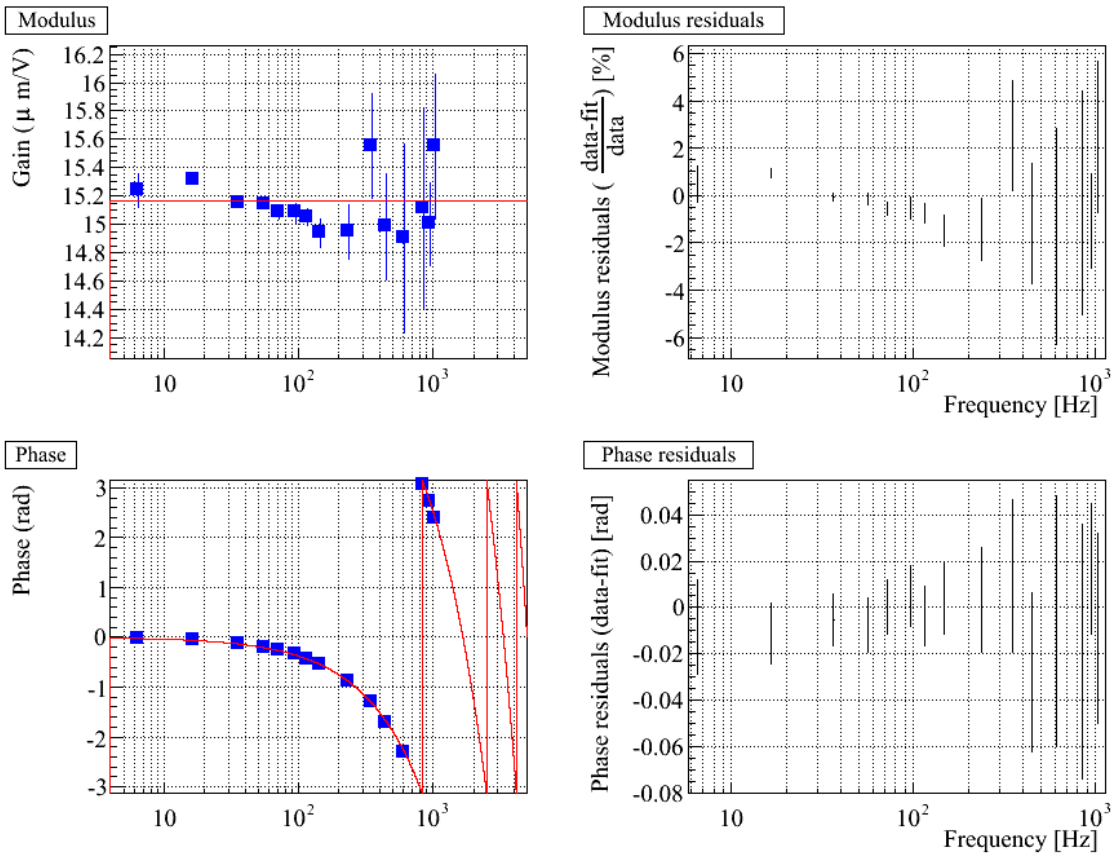

Figure 14: ***Measured actuation of the WE mirror using the L-R coils in LN1 mode****, fitted model and residuals.*

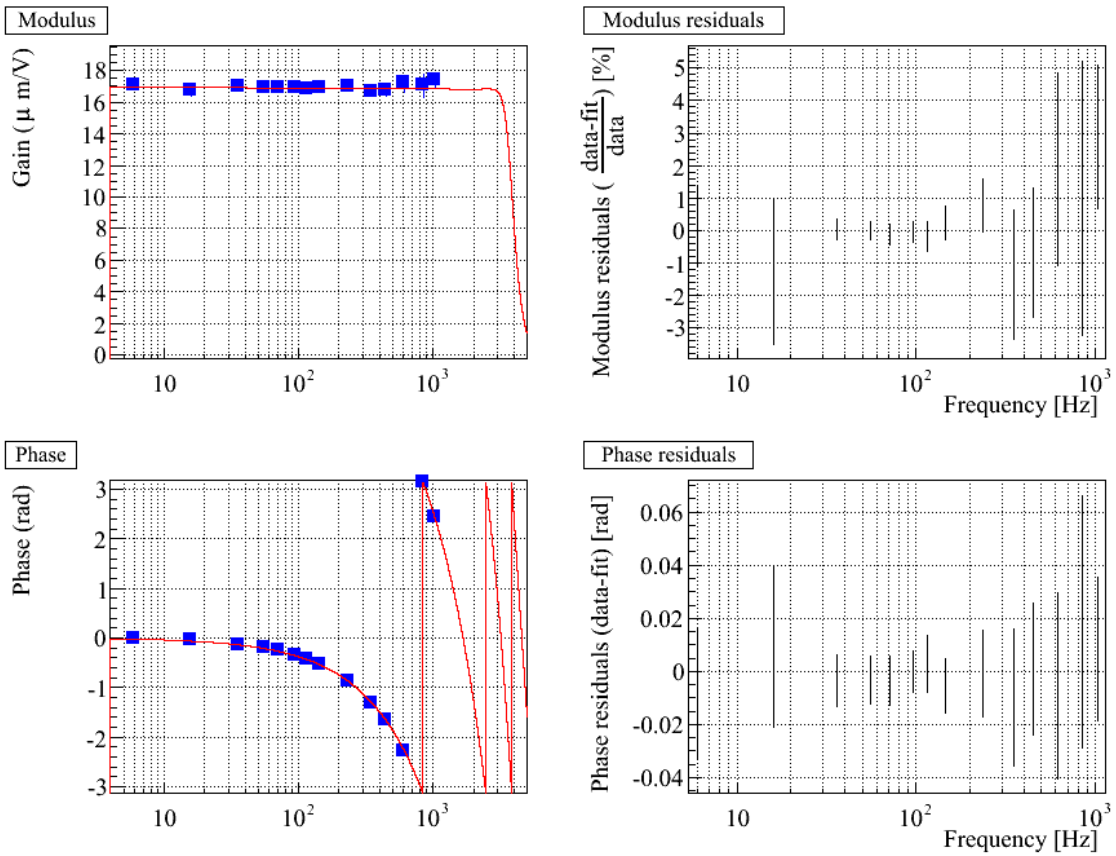

Figure 15: ***Measured actuation of the NE mirror using the U-D coils in LN1 mode****, fitted model and residuals.*

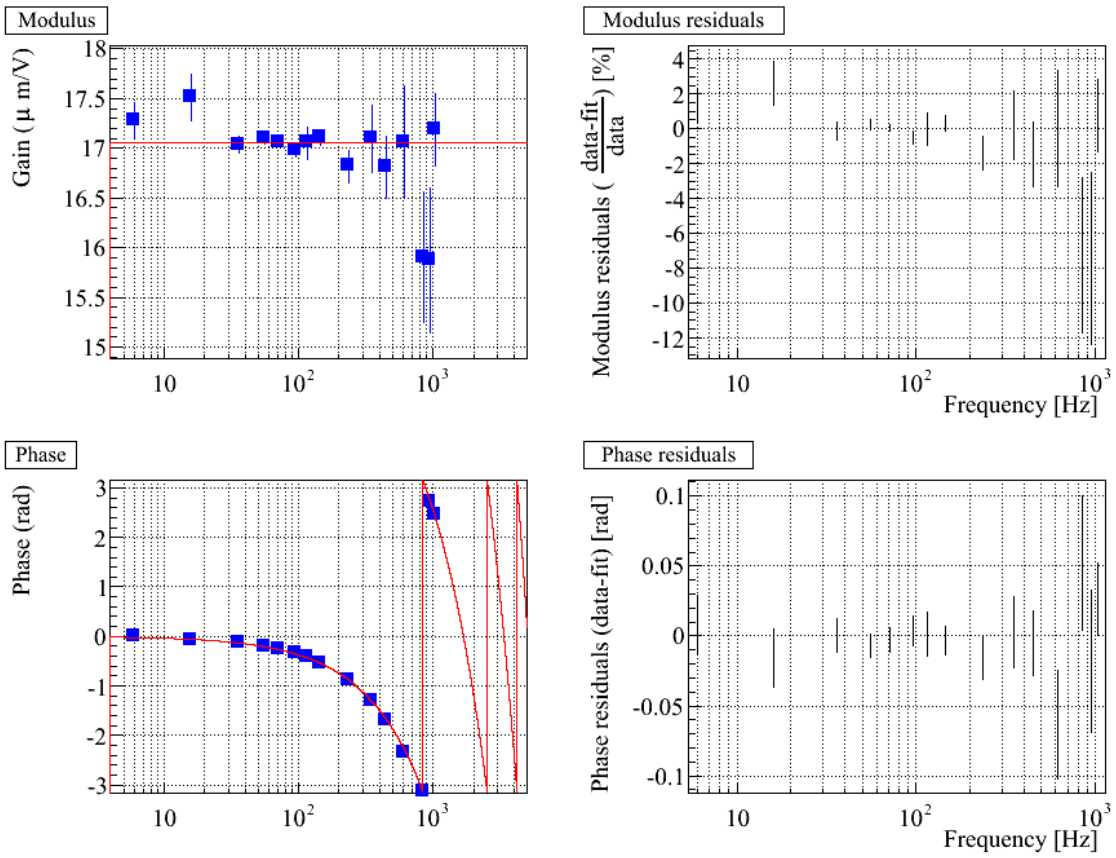

Figure 16: ***Measured actuation of the NE mirror using the L-R coils in LN1 mode****, fitted model and residuals.*

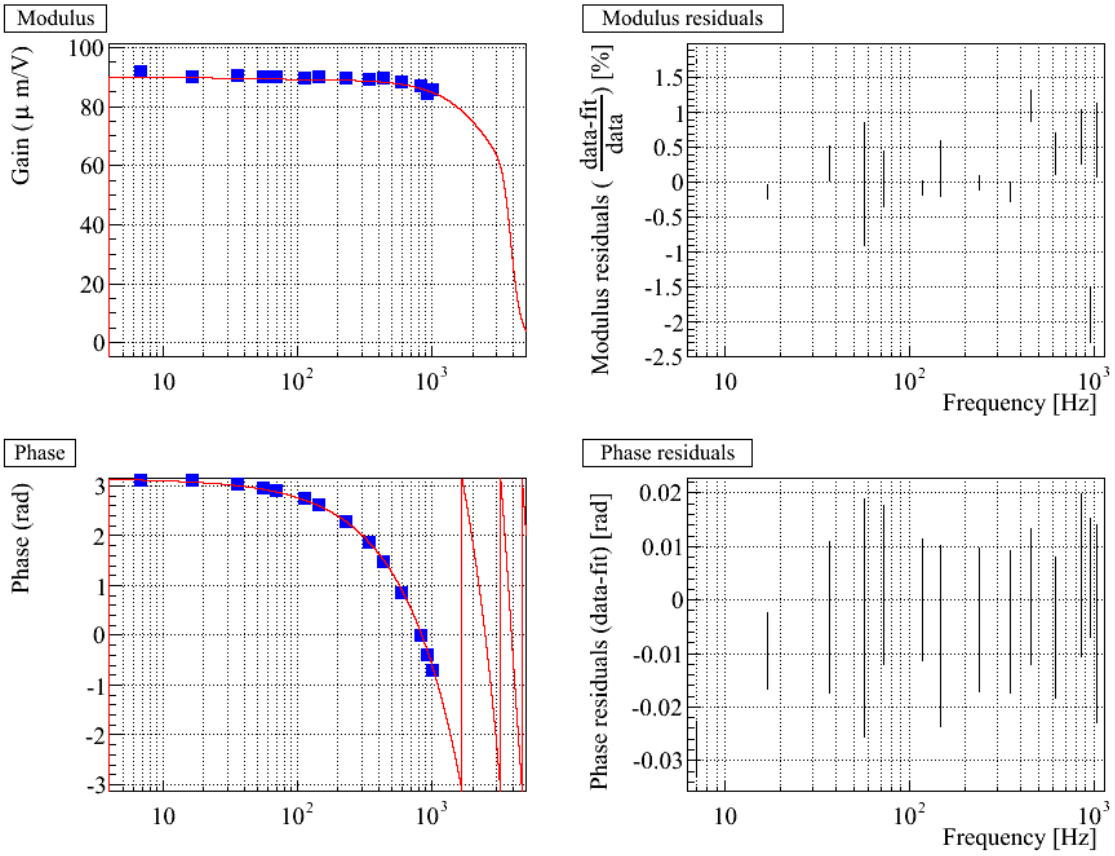

Figure 17: ***Measured actuation of the BS mirror using the four coils in LN1 mode****, fitted model and residuals.*

4 Calibration of the marionette actuation

The marionette actuation is defined as the TF (with modulus in m/V) from the correction signal to the induced mirror motion[11] (i.e. Sc_WE, NE_zM). The time reference is the GPS time.

In the plots that are shown, the actuation is corrected for the mechanical model of the pendulum, defined as **two** 2nd order low-pass filters with $f_0 = 0.6\,\mathrm{Hz}$ and $Q = 1000$.

4.1 Description of the measurements

The calibration of the NE (U-D coils) and WE (U-D coils) mirror actuation in LN1 mode is used as reference to measure the NE and WE marionette actuations.

An intermediate step consists in measuring the Marionette/Mirror TF ratio. This is performed using the ITF in step 12, and measuring the ITF response in closed loop in two datasets:

- one injecting noise to the mirror actuation. It permits to measure the ITF response R_1 as function of the injected signal, in W/V,
- one injecting noise to the marionette actuation. It permits to measure the ITF response R_2 as function of the injected signal, in W/V.

Then, the ratio of R_2/R_1 gives the ratio of the responses of the marionette actuation to the mirror actuation. This ratio is then multiplied by the model of the mirror actuation (U-D coils, in LN1 mode) to obtain the marionette actuation. Only the points where the coherence is higher than 80% have been used to estimate R_1 and R_2.

This analysis assumes that the ITF response (in particular the optical gain) is stable between the two datasets. In principle this is the case since both datasets are taken within 3 minutes[12]. It will be checked monitoring the ratio during the run.

The injected noise has been white noise from a few Hz to ~ 200 Hz.

4.2 Calibration of the WE and NE marionettes

The measured ratio of the WE and NE marionette to mirror responses are shown figures 18 and 20 (the mirror and marionette actuations being corrected for their pendulum mechanical model).

[11] The marionette longitudinal actuation is done through two coils (left and right). Emphasis filters are set in the DSP for both coil channels in order to compensate for de-emphasis filters used in the coil drivers. The resistance of the coil channel is $R \sim 16.5\,\Omega$ and its inductance is $L \sim 214\,\mathrm{mH}$: the L-R circuit results in a pole $R/(2\pi L)$ around $12 - -13\,\mathrm{Hz}$.

[12] This hypothesis was valide during VSR2.

The obtained marionette TF is shown figures 19 and 21 along with the fitted model and residuals. The fits were performed between 9 Hz and 200 Hz for WE and 10 Hz to 100 Hz for NE. The fit parameters are given in the table 5. Below 100 Hz, the residuals are flat, lower than 15% in modulus and better than 150 mrad in phase.

Note that the 4 μs timing systematic error are negligible for the marionettes: at 100 Hz, it corresponds to less than 3 mrad phase error.

4.3 Tables

	WE	NE
Gain (μm/V)	2.792 ± 0.027	3.140 ± 0.029
Raw delay (μs)	(-747 ± 133)	(5.3 ± 2.7)
Delay (μs)	-896.3 ± 133	-144 ± 2.7
Φ_0 (rad)	0	0
Pole frequency (Hz)	16.86 ± 0.36	14.39 ± 0.24
Zero frequency (Hz)	90.8 ± 23	68.2 ± 9.5
Pole frequency (Hz)	74.30 ± 17	75.3 ± 9.5
Complex zero f_0 (Hz)	-244.1 ± 34	-337.4 ± 35
Complex zero Q	0.526 ± 0.035	0.85 ± 0.08
Pendulum	**Two** 2nd order low-pass filters: $f_0 = 0.6\,\mathrm{Hz}$, $Q = 1000$	
χ^2/ndf	1652.5/1825	1184.6/1431

Table 5: ***WE and NE marionette actuation parameterizations.*** *Fit computed from 9 Hz to 200 Hz on WE and from 10 Hz to 100 Hz on NE. The χ^2/ndf of the fits are given. Residuals are within 15% in modulus and 150 mrad in phase up to 100 Hz. The raw delays are the delay measured using the raw delays from the mirror actuation measurements. The delay has been corrected for the PrCa and sensing delays to take as reference the correction channels (i.e. Sc_WE_zM): $delay = raw\_delay - 100 - 49.3$ μs. Applying these TFs to the correction channels Sc_WE_zM should enable to estimate the induce motion at absolute GPS time.*

4.4 Figures

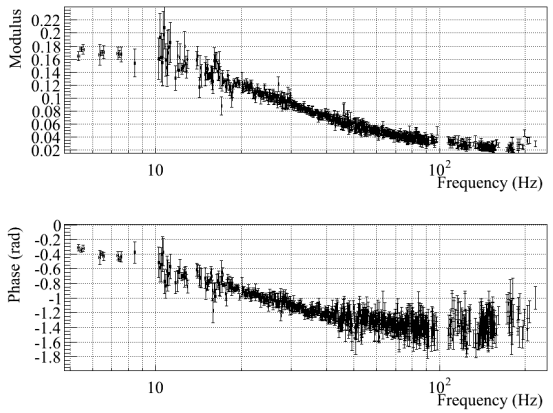

Figure 18: ***Averaged marionette to mirror actuation TF ratio of the WE suspension.*** *The mirror and marionette actuations have been corrected for their pendulum mechanical models.*

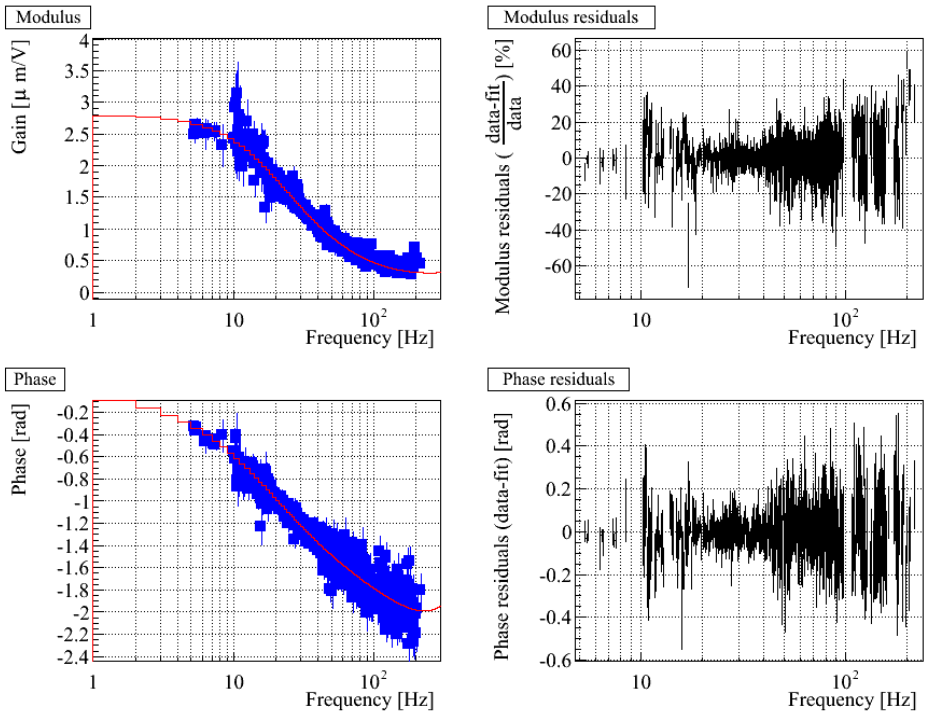

Figure 19: ***Measured WE marionette actuation TF****, fit and residuals.*

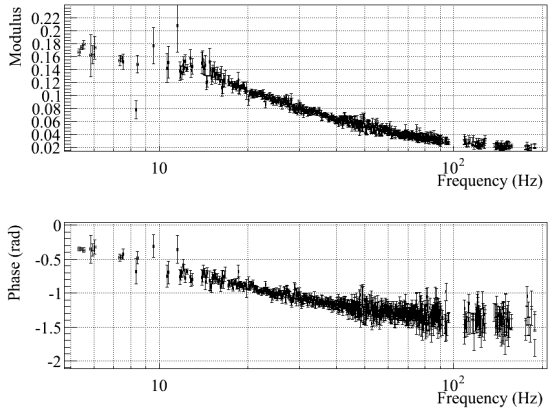

Figure 20: ***Averaged marionette to mirror actuation TF ratio of the NE suspension.***

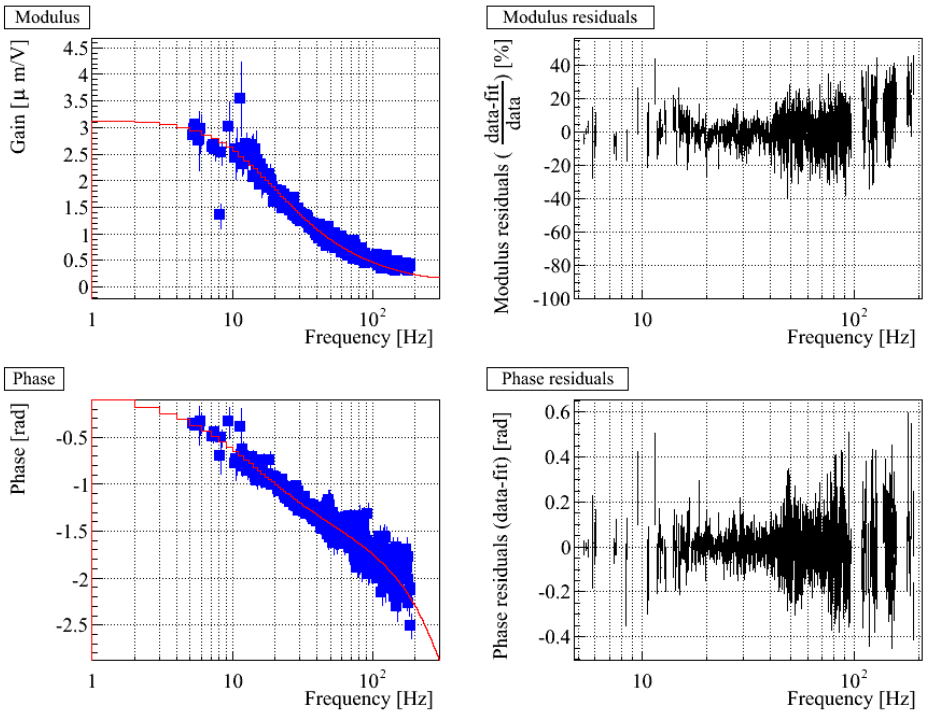

Figure 21: ***Measured NE marionette actuation TF****, fit and residuals.*

5 Conclusions

The preliminary parameterizations of the sensing and mirror and marionette actuation responses given in this note have been estimated from few data between June 19th and August 4th 2010, before the start of VSR3.

The first calibration for VSR2 has been computed with data from June 28th to September 1st 2009, including pre-run measurements and run periodic measurements.

The dark fringe readout has been calibrated, the timing being related to the absolute GPS time. The timing has been computed from the time series stored in FrVect setting the value of sample i at the time $startX[0] + i \times dx[0]$. The 20 kHz dark fringe channel models, given in the table 1, are understood from 1 Hz to 10 kHz within systematic errors of ± 4 μs. The sensing did not change since VSR2.

The mirror actuation in LN1 mode has been measured from 5 Hz to $\sim$1 kHz. The parameterizations are given in the tables 3 for the controls and 4 for the hardware injections. The delays are related to the absolute GPS time. Systematic errors are estimated to 5% in modulus and 50 mrad/10 μs in phase/timing. No time has been allocated to check the linearity of the actuation response. It will be done after the run. A weekly monitoring of the response will be done during VSR3.

The PR mirror actuation has not been measured, but no change is expected since VSR2 and the parameterization from [2] should still be valid.

The marionette actuation responses have been measured from 9 Hz to 200 Hz. The parameterizations are given in the table 5 for WE and NE. The delays are related to the absolute GPS time. Statistical errors are of the order of 15%/150 mrad in modulus and phase respectively. The linearity of the response has not been checked. A weekly monitoring of the response will be done during VSR3.

Online status - The sensing and mirror parameterizations presented in this note are used for the start of VSR3 in the following online processes:

- the sensitivity and horizon computation,
- the hardware injections and the blind injections,
- the h(t) reconstruction[13].

[13] For the marionette actuation response, note that the h(t) reconstruction still (on August 4th 2010) uses the parameterizations defined for VSR2 [2].

References

[1] L. Rolland *Calibration status in September 2009* (2009) VIR-0576A-09.

[2] L. Rolland *VSR2 mirror and marionette actuator calibration* (2010) VIR-0076B-10.

[3] L. Rolland, F. Marion, B. Mours, *Mirror and marionette actuation calibration for VSR1* (2008) VIR-015A-08.

[4] A. Gennai, private discussion 2006

A Dark fringe ADC configuration

B Filter definitions

The definitions of the different filters used in the calibration prameterizations are given in this appendix.

B.1 Simple pole

A pole at frequency f_p is described as:

$$H(f) = \frac{1 - \mathrm{j}x}{1 + x^2}$$

where $x = \frac{f}{f_p}$.

The frequency f_p should be positive to have a stable filter.

B.2 Simple zero

A zero at frequency f_0 is described as:

$$H(f) = 1 + \mathrm{j}x$$

where $x = \frac{f}{f_0}$.

B.3 2nd order low-pass filter (complex pole)

A 2nd order low-pass filter at frequency f_0 with quality factor Q is described by:

$$H(f) = \frac{-f_0^2(f^2 - f_0^2) - \mathrm{j}\frac{f_0^3 f}{Q}}{(f^2 - f_0^2)^2 + (\frac{f f_0}{Q})^2}$$

The frequency f_0 should be positive to have a stable filter.

B.4 Complex zero

A complex zero at frequency f_0 with quality factor Q is described as the inverse of a 2nd order low-pass filter:

$$H(f) = \frac{1}{\frac{-f_0^2(f^2 - f_0^2) - \mathrm{j}\frac{f_0^3 f}{Q}}{(f^2 - f_0^2) + (\frac{f f_0}{Q})^2}}$$

B.5 8th order Butterworth filter

A 8th order Butterworth filter with a cut-off frequency f_0 is defined as:

$$H(s) = \frac{1}{(s^2 + 0,3902s + 1)(s^2 + 1,1111s + 1)(s^2 + 1,6629s + 1)(s^2 + 1,9616s + 1)}$$

where $s = \mathrm{j} \times \frac{f}{f_0}$.

B.6 Anti-alias of the DAC in the mirror actuation

The parameters[14] of the DAC anti-alias are given in the table 2. The absolute sign of z_1, p_1, p_2, p_4, p_6 and p_7 is important (they are all negative). The sign of the other pulsations is not important in the computation since they are squared.

The TF can be written $H(w) = \frac{N(w)}{D(w)}$ with:

$$\begin{aligned}
N(w) &= (1 - \mathrm{j}\frac{\omega}{z_1}) && (1)\\
&\times(1 - \frac{\omega^2}{z_2^2}) \quad \text{(it describes a notch)} && (2)\\
&\times(1 - \frac{\omega^2}{z_3^2}) && (3)\\
&\times(1 - \frac{\omega^2}{z_4^2}) && (4)\\
D(w) &= (1 - \mathrm{j}\frac{\omega}{p_1}) && (5)\\
&\times(1 - \frac{\omega^2 - \mathrm{j} \times 2p_2\omega}{p_2^2 + p_3^2}) && (6)\\
&\times(1 - \frac{\omega^2 + \mathrm{j} \times 2p_4\omega}{p_4^2 + p_5^2}) && (7)\\
&\times(1 - \frac{\omega^2 + \mathrm{j} \times 2p_6\omega}{p_6^2 + p_7^2}) && (8)\\
&\times(1 - \mathrm{j}\frac{\omega}{p_8}) && (9)
\end{aligned}$$

[14] They have been given by Alberto Gennai.